

Experimental investigation and thermodynamic calculation of the B-Fe-W ternary system

Xuemei OuYang^{a,b}, Fucheng Yin^{a,b,*}, Jingxian Hu^{a,b}, Manxiu Zhao^{a,b}, Ye Liu^{a,b}, Faguo Li^{a,b}

^a School of Materials Science and Engineering, Xiangtan University, Xiangtan, Hunan 411105, PR China

^b Key Laboratory of Materials Design and Preparation Technology of Hunan Province, Xiangtan University, Xiangtan, Hunan 411105, PR China

ARTICLE INFO

Keywords:

B-Fe-W system
Liquidus projection
Thermodynamic modeling
Phase diagram

ABSTRACT

The ternary B-Fe-W system is of interest for the wear resistant applications. Its liquidus projection in the Fe-rich region was experimentally determined and thermodynamic modeling was performed in this work. The microstructures of the solidified samples were observed by scanning electron microscopy, the compositions of the primary crystallization phases were obtained by electron probe microanalysis, and the reaction temperatures were determined by differential scanning calorimetry. The observed primary solidification phases are BCC (Fe), FCC, WFeB, Fe₂B, μ , and BCC (W), respectively. A thermodynamic model of the B-Fe-W system based on thermodynamic models of the three constituent binary systems and the experimental results for the ternary system was developed using the CALPHAD approach. A set of self-consistent thermodynamic parameters for the B-Fe-W system was obtained and reasonable agreement between the experimental and calculated isothermal sections and liquidus projection was obtained.

1. Introduction

Borides, especially transition metal borides, are potentially excellent candidates for wear resistant applications owing to their unique combination of high hardness, a high melting point, and relatively high electrical conductivity among hard materials [1]. Conventional ternary borides such as Mo₂FeB₂, Mo₂NiB₂ and WC₀B have been investigated intensively in the last several decades [2], and have been employed widely in wear resistant applications, for instance, injection molding machine parts, can forming tools, and dies for the extrusion of copper. In light of the bright prospect for ternary borides, a type of transition metal boride WFeB, which possesses the superior properties of transition metal boride, was prepared and investigated recently. Its excellent thermal stability and high theoretical density (13.27 g/cm³) are impressive, and WFeB is expected to be used in wide range of applications, e.g. hard materials, wear-resistant materials, and heat-resistant materials [3–5].

Knowledge of the phase relations and thermodynamic modeling are important for designing alloy compositions and processing methods. In this work, solidified alloys of the Fe-rich region were experimentally investigated using SEM, EPMA, DSC, and XRD to determine the species of the primary phases, the invariant reactions, and phase transformations during solidification. In addition, thermodynamic optimization of the ternary system based on thermodynamic descriptions of the three

constituent binary systems and the experimental results for the ternary system was carried out using the CALPHAD method.

2. Review of literature

2.1. Binary systems

The equilibrium phases in the B-Fe binary system are the liquid (L), BCC (α -Fe and δ -Fe), FCC (γ -Fe), rhombohedral B (β B), Fe₂B, and FeB phases. In addition, Khan et al. [6] reported the formation of the metastable Fe₃B phase in the rapidly quenched samples, whereas Battrezzati et al. [7] reported that Fe₃B can be stabilized by the reaction, $Fe_3B \rightleftharpoons Fe_2B + \alpha$ -Fe. Many thermodynamic descriptions of the B-Fe system have been extensively reported [8–12]. More recently, Yoshitomi et al. [10] reassessed the B-Fe system by combining first principles calculations and the CALPHAD method. However, the invariant reaction temperature of L \rightleftharpoons FeB + (β B) predicted in their work is approximately 43 °C lower than the widely accepted value of 1500 °C. The thermodynamic parameters assessed by Palumbo et al. [12] were adopted, because the calculated results are in good agreement with the experimental data. The calculated phase diagram is shown in Fig. 1a.

The phase equilibria of the B-W system were recently summarized by Duschanek and Rogl [13], and a thermodynamic assessment of this system was also conducted in their work. Five compounds in this

* Corresponding author at: School of Materials Science and Engineering, Xiangtan University, Xiangtan, Hunan 411105, PR China.

E-mail address: fuchengyin@xtu.edu.cn (F. Yin).

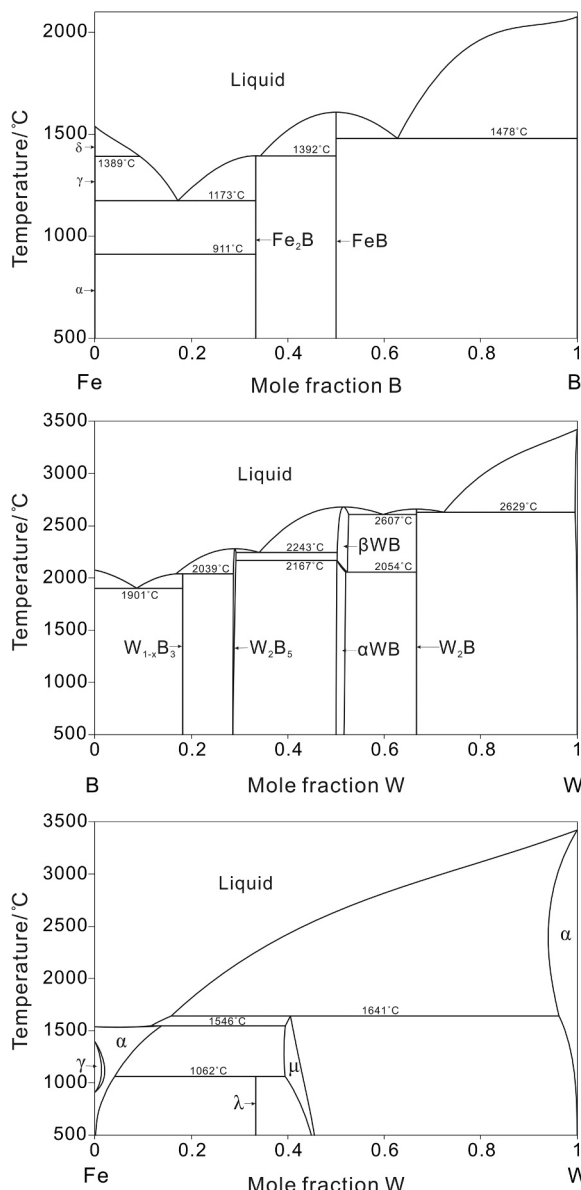


Fig. 1. Calculated binary phase diagrams (a) Fe-B system [12]; (b) W-B system [13]; (c) Fe-W system [20].

system, $W_{1-x}B_3$, W_2B_5 , αWB , βWB , and WB , were considered to be stable. βWB changes to αWB through a eutectoid reaction at 2054 °C. $W_{1-x}B_3$ is stable below 2020 °C [14]. The calculated B-W phase diagram is shown in Fig. 1b.

The equilibrium phase diagram of the Fe-W system was firstly proposed by Sykes et al. [15]. Many experimental investigations and thermodynamic assessments were subsequently conducted [16–20]. Recently, the thermodynamic assessment of this binary system adopted in this work was made by Jacob et al. using the first-principle calculation method [20]. Fig. 1c shows the calculated Fe-W phase diagram, in which only two intermediate phases, μ and λ , are included in the system.

2.2. B-Fe-W ternary system

Only a few experimental studies of the B-Fe-W ternary system have been reported. Haschke et al. [21] proposed the isothermal section at 1000 °C on the basis of the results obtained from samples with annealing times of 3 weeks. Three ternary solid phases were confirmed to

be stable at 1000 °C, τ_1 -WFeB with TiNiSi-type structure, τ_2 -W₂FeB₂ with W₂CoB₂-type structure, and $W_{0.7}Fe_{0.15}B$ phase with CrB-type structure, respectively. The existence of $W_{0.7}Fe_{0.15}B$ is controversial because βWB can be stable only above 2054 °C. Further, it was considered a non-equilibrium phase in the recent review by Rogl et al. [22]. Thus, $W_{0.7}Fe_{0.15}B$ should be removed from the 1000 °C isothermal section. In addition, the $W_{1-x}B_3$ phase can be stable below 2020 °C and should be added. The isothermal section at 1050 °C was constructed by Leithe-Jasper et al. [23] using X-ray powder diffraction without considering the solubilities of the compounds. τ_1 -WFeB and τ_2 -W₂FeB₂ were confirmed to be stable at 1050 °C. A metastable phase (W_xFe_{1-x})₃B, $x \approx 0.2$, with the same structure as Fe_3B was found in the alloy (Fe-0.05W-0.25B) after annealing at 1100 °C for 14 days, but it was not considered in the 1050 °C isothermal section. Fe_3B usually adopts the Fe_3C type at the temperature below 1214 °C, and it also can be found in Ti_3P type at a limited temperature range. On the basis of the above analysis, the two isothermal sections were amended, as shown in Fig. 2. The available crystallographic data of all the compounds in the B-Fe-W system are summarized in Table 1.

No thermodynamic description of this ternary system is available. Therefore, a more reliable assessment of the system should be undertaken on the basis of these literature data and the results obtained from the present work.

3. Experimental methods

3.1. Sample preparation

Twenty-three ternary B-Fe-W alloys with varying B and W contents were prepared, including nineteen alloys for determination of the liquidus projection and three alloys for the vertical section with B fixed at 3.5 wt%. Melting was attempted using pieces of Fe, W, and FeB in a non-consumable vacuum arc-melting furnace, however, it failed owing to the high melting point of W, as a result of which W particles were deposited at the bottom of the sample. Thus, all the samples were prepared from powder compacts, and then sealed in an evacuated quartz tube. The purity of the power materials (Fe, W, B) was 99.99 wt%. Each sample was initially held at a constant temperature of 800 °C for 12 h, and then held at 1100 °C for 48 h. The samples were quenched with water at the end of the heating sequence, and finally were re-melted in a high-purity argon atmosphere using a non-consumable vacuum arc-melting furnace. The solidified alloys (5–7 g) were melted at least four times to achieve homogeneity. The nominal compositions of the alloys are given in Table 2.

3.2. Microstructure and chemical composition analyses

A JEOL JEM-6360LV scanning electron microscope was used for microstructure analysis. The chemical compositions of the primary phases in the alloys were determined by a JEOL 8630LV electron probe microanalyzer.

3.3. XRD and DSC

The coexisting phases in each alloy were further identified using XRD analysis (Rigaku Ultima IV) with Cu K α radiation from a Ni-crystal monochromator. The operating voltage and current were 40 kV and 40 mA, respectively. The melting behavior and solidification path were determined by differential thermal analysis (DSC-NETZSCH 404F) during slow cooling (5 K/min). DSC experiments were performed on samples in Al₂O₃ crucibles under a continuous flow of argon (99.998% purity). Data for the solid-state phase transition temperatures were obtained from the heating curves, and the liquidus temperatures were taken from the cooling curves. To obtain accurate values, each sample was tested three times. Owing to the overlap of the peaks in the heating curves, the signals obtained during cooling were used to evaluate the

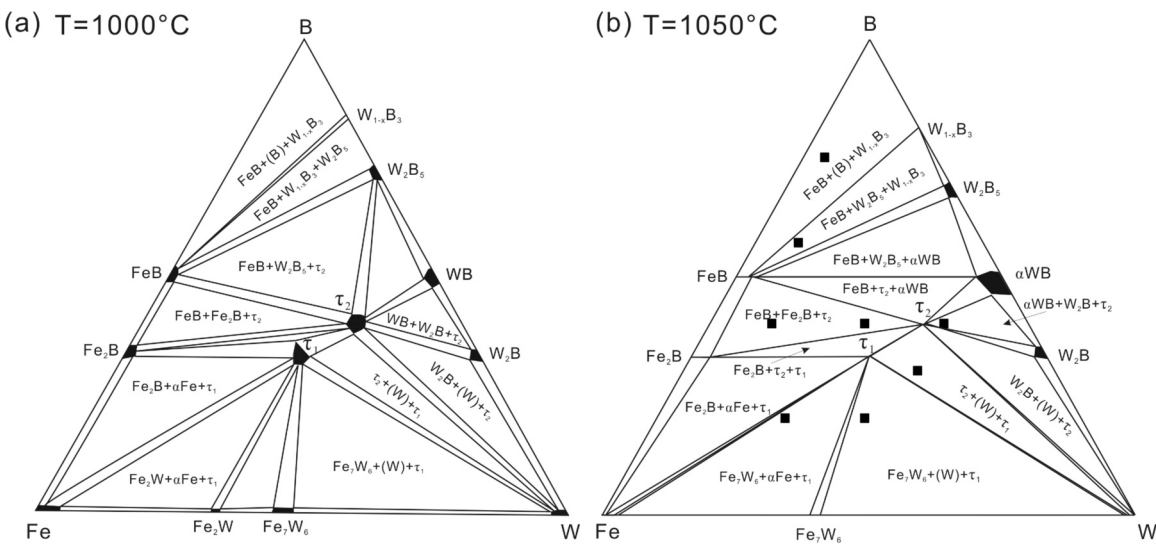


Fig. 2. (a) Amended isothermal section at 1000 °C; (b) amended isothermal section at 1050 °C.

Table 1
Crystallographic data and enthalpy of the binary and ternary compounds.

Phase	Pearson symbol	Proto-type	Space group	Lattice parameters(nm)			Enthalpy (kJ/mol)
				a	b	c	
FeB	oP8	FeB	<i>Pnma</i>	0.5506 ^[27]	0.2952	0.4061	- 35.6 ± 6.3 ^[30] , - 46.5 ^[31] , - 32.3 ± 2.2 ^[32]
				0.54082	0.2949	0.3998	- 35.99 ^[O*]
Fe ₂ B	tI12	CuAl ₂	<i>I4/mcm</i>	0.5110 ^[27]	0.4240	- 22.3 ± 7.0 ^[30] , - 33.8 ^[31] , - 22.6 ± 2.7 ^[32]	
				0.5062	0.4233	- 30.2 ^[O*]	
Fe ₃ B	tI32	Ti ₃ P	<i>P4₂/n</i>	0.5428 ^[27]	0.6669	0.4439	- 21.84 ^[O*]
				0.5406	0.6661	0.4363	- 87.0 ± 16.7 ^[33] , - 66.9 ± 9.2 ^[34]
W ₂ B	tI12	CuAl ₂	<i>I4/mcm</i>	0.5567 ^[28]	0.4744	- 70.36 ^[O*]	
				0.5592	0.4797	- 66.1 ^[34] , - 66.9 ^[35] , - 63.7 ^[13]	
αWB	tI16	αWB	<i>I41/amd</i>	0.3100 ^[28]	1.6955	- 71.02 ^[O*]	
				0.3146	1.7044	- 54.5 ^[13]	
βWB	oC8	CrB	<i>Cmcm</i>	0.3124 ^[28]	0.8445	0.3060	- 68.50 ^[O*]
				0.3187	0.8515	0.3110	- 199.6 ^[36] , - 122.5 ^[37]
W ₂ B ₅ (h)	hP12	W ₂ B _{5-x}	<i>P6/mmc</i>	0.2982 ^[28]	1.3873	- 178.29 ^[O*]	
				0.3102	1.4290	- 176.26 ^[O*]	
W ₂ B ₅ (r)	hR21	W ₂ B _{5-x}	<i>R-3 m</i>	0.3011 ^[28]	2.093	- 156.9 ^[38] , - 82.5 ^[13]	
				0.3099	2.1468	- 76.8 ^[O*]	
W _{1-x} B ₃	hP20	W _{1-x} B ₃	<i>P63/mmc</i>	0.5200 ^[28]	0.6340	- 62.262 ^[O*]	
				0.5366	0.6470	- 55.746 ^[O*]	
μ-W ₆ Fe ₇	hR39	W ₆ Fe ₇	<i>R-3 m</i>	0.4759 ^[28]	2.5715		
λ-Fe ₂ W	hP12	MgZn ₂	<i>P63/mmc</i>	0.4737 ^[28]	0.7719		
W ₂ FeB ₂	oI10	W ₂ CoB ₂	<i>Imm</i>	0.7125 ^[28]	0.4611		
				0.5754	0.3173		
WFeB	oP12	TiNiSi	<i>Pnma</i>	0.5823 ^[29]	0.3161	0.6810	
				0.5704	0.3258	0.6664	

O*- Calculated values in this work.

liquidus temperature even if the potential for supercooling could not be avoided.

4. Experimental results

Nineteen as-solidified alloys were prepared to obtain the proposed liquidus projection of the B-Fe-W ternary system in the Fe-rich region. The nominal compositions and the compositions of the primary phase in each sample are given in [Table 2](#).

Fig. 3a shows the microstructure of alloy A1, in which the primary phase is dendritic α -Fe. Similar results are obtained for alloys A2 and A3. **Fig. 3b** is a back-scattered electron image (BEI) micrograph of as-solidified alloy A4 (Fe-15 at% B-15 at% W). It comprises the matrix α -Fe phase, the gray block Fe_3B phase, binary eutectic microstructure (α -Fe + WFeB), and small net-like eutectoid microstructure (Fe_3B + α -Fe). The primary phase is γ -Fe, which transforms into α -Fe at 912 °C. **Fig. 3c** shows the

microstructure of alloy A5, in which the primary phase is a large block of Fe₂B. The compositional analysis indicated that approximately 2 at% of W was dissolved in Fe₂B. The primary solidification field of ternary phase WFeB is large and the results were obtained from alloys A7, A8, A9, A10, A11, and A12. The microstructures of alloys A7 and A11 are shown in Figs. 3d and 3e, respectively. The compositional analysis and XRD results confirmed that the primary phases in alloys A13, A14, A15, A16, and A17 are light gray μ with little dissolved B. Figs. 3f-3h are BEI micrographs of as-solidified alloys A13, A14, and A15, respectively. Fig. 3i shows the microstructure of alloy A18. The primary phase in alloy A18 is white (W) and is surrounded by the light gray μ phase, which is a typical microstructure formed by a peritectic reaction.

Fig. 4b is a back-scattered electron image (BEI) micrograph of as-solidified alloy A10 (Fe-15 at% B-15 at% W). Three phases were observed. The bright phase is WF₆B, the gray phase is Fe₃B, and the dark phase is α -Fe. The existence of these three phases is confirmed by the

Table 2

Alloy compositions and primary phases of the ternary B-Fe-W alloys.

Alloy	Composition (at%)			Primary phase	Primary Phase Composition (at%)		
	Fe	B	W		Fe	B	W
A1	85	10	5	BCC	96.8	–	3.2
A2	80	10	10	BCC	96.1	–	3.9
A3	75	10	15	BCC	96.9	–	3.1
A4	80	15	5	FCC	94.8	–	5.2
A5	75	22	3	Fe ₂ B	65.2	32.7	2.1
A6	70	27	3	Fe ₂ B	64.6	33.1	2.3
A7	75	20	5	WFeB	32.6	34.2	33.2
A8	70	22	8	WFeB	32.9	33.8	33.3
A9	70	20	10	WFeB	32.7	32.9	34.4
A10	75	15	10	WFeB	32.8	34.0	33.2
A11	70	15	15	WFeB	33.2	33.2	33.6
A12	65	15	20	WFeB	33.0	33.9	33.1
A13	80	5	15	μ	56.8	–	43.2
A14	80	3	17	μ	57.5	–	42.5
A15	75	5	20	μ	58.2	–	41.8
A16	70	10	20	μ	56.9	–	43.1
A17	65	10	25	μ	56.6	–	43.4
A18	75	3	22	BCC	5.7	–	94.3
A19	70	5	25	BCC	5.3	–	94.7

XRD results, as shown in Fig. 4a. According to the DSC results and microstructures, it can be concluded that solidification starts with the formation of WFeB, continues with the binary eutectic reaction at 1393 °C ($L \leftrightarrow \alpha\text{-Fe} + \text{WFeB}$), and concludes with a ternary eutectic reaction ($L \leftrightarrow \tau_1 + \text{Fe}_2\text{B} + \gamma\text{-Fe}$) at 1156 °C. Fig. 5b is a BEI

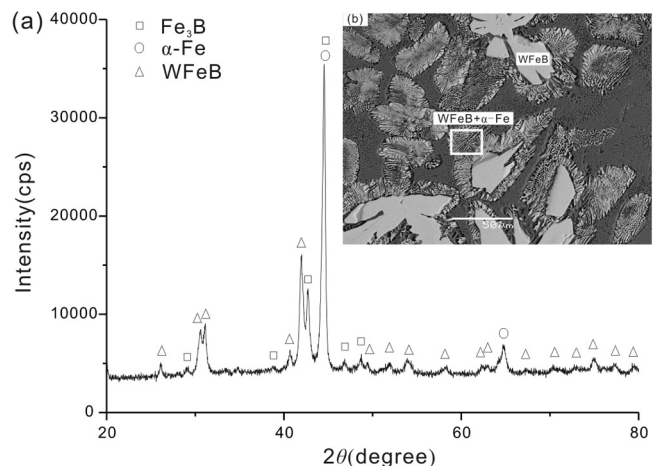


Fig. 4. (a) XRD patterns and (b) microstructure of alloy A10 (Fe-15 at% B-10 at% W).

micrograph of as-solidified alloy A16 (Fe-10 at% B-20 at% W). Three different phases regions were observed. The bright phase is μ, the finer dendritic phase is WFeB, and the dark phase is α-Fe. The existence of these three phases is confirmed by the XRD patterns, as shown in Fig. 5a. The solidification begins with the formation of the intermetallic phase μ. Then solidification may continue with a binary peritectic reaction ($L + \mu \leftrightarrow \alpha\text{-Fe}$) at 1485 °C, follows by an invariant reaction ($L \leftrightarrow \mu + \text{WFeB} + \alpha\text{-Fe}$) at 1365 °C.

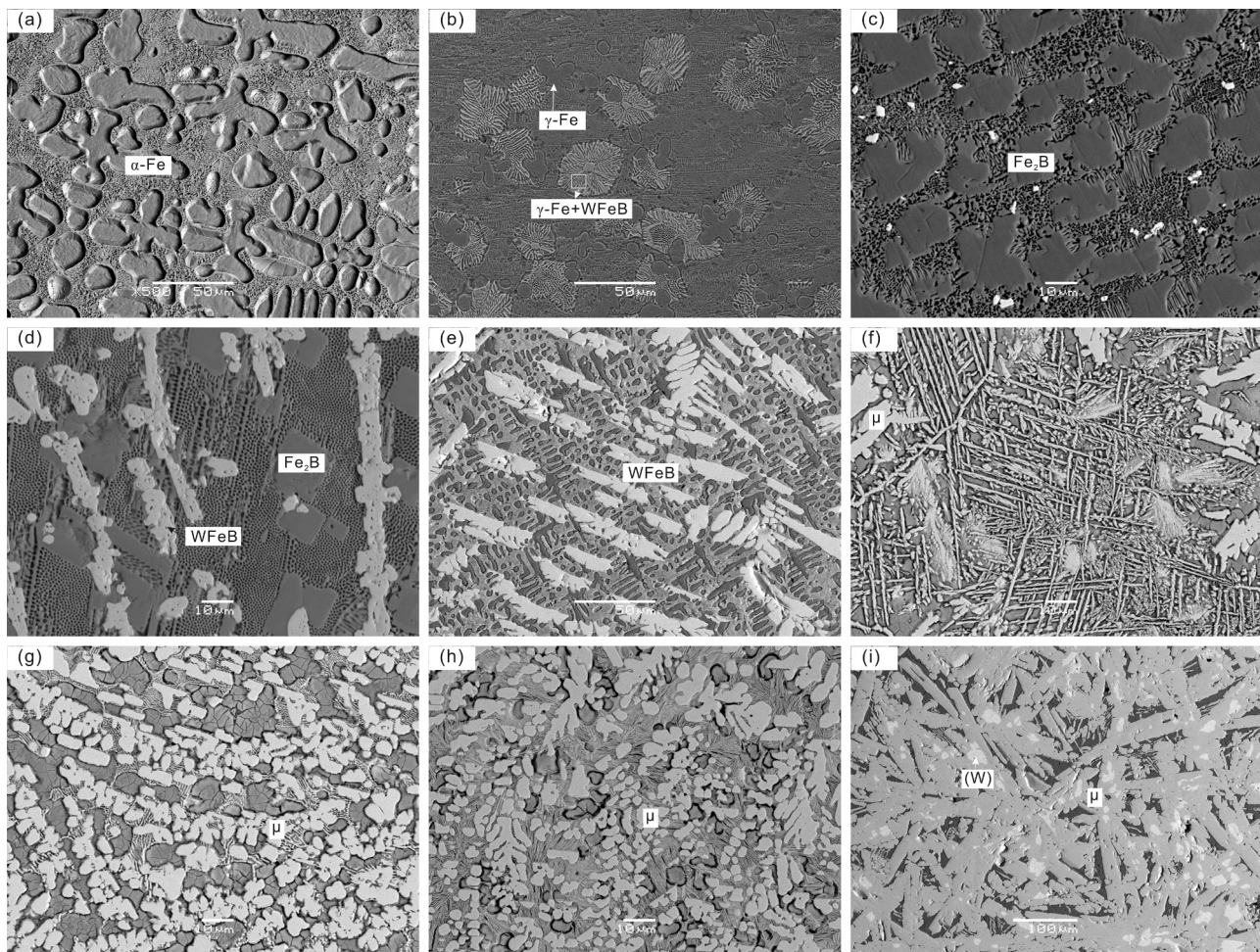


Fig. 3. Microstructures of some typical alloys (a) A1; (b) A4; (c) A5; (d) A7; (e) A11; (f) A13; (g) A14; (h) A15; and (i) A18.

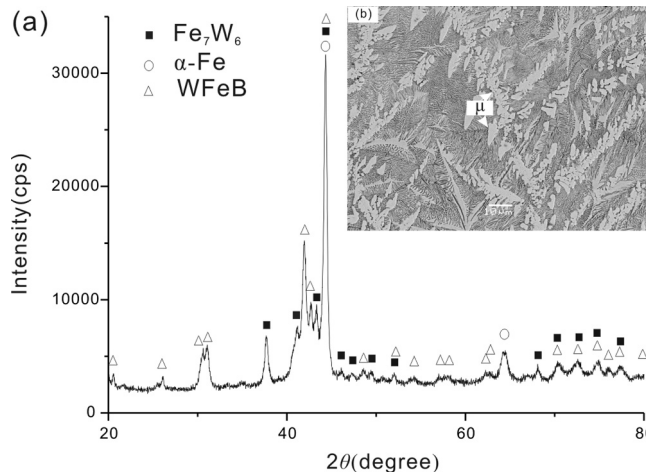


Fig. 5. (a) XRD patterns and (b) microstructure of alloy A16 (Fe-10 at% B-20 at % W).

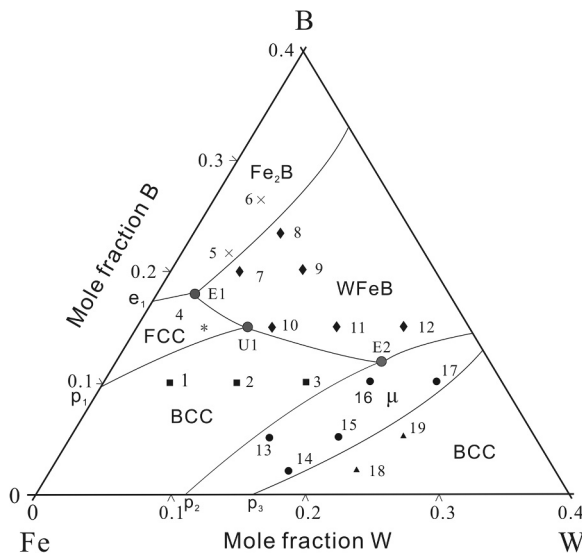


Fig. 6. Liquidus projection of the B-Fe-W system in the Fe-rich region.

The liquidus projection of the B-Fe-W system in the Fe-rich region was proposed according to the results obtained from this work and the phase diagrams of the constituent binary systems, as shown in Fig. 6. This liquidus projection shows six primary solidification surfaces, FCC, two types of BCC, WFeB, Fe₂B, and μ. These primary solidification surfaces are separated by the appropriate curves for joint crystallization resulting in three four-phase invariant equilibria. Three four-phase invariant reactions are conducted: two eutectic types, $L \leftrightarrow \tau_1 + Fe_2B + FCC$ and $L \leftrightarrow \mu + WFeB + BCC$ and one quasi-peritectic type, $L + BCC \leftrightarrow \tau_1 + FCC$.

5. Thermodynamic modeling and calculation results

5.1. First-principle calculations of the borides involved in the ternary system

First-principles calculations based on density functional theory, one of the most accurate methods for precise calculation of the total energies of solids, has been widely used to investigate the stability of compounds [24]. To improve the thermodynamic assessment, it was employed in this work using the generalized gradient approximation to

obtain reliable values of the enthalpy of formation [25]. The valence electrons were explicitly treated as projector augmented plane-wave potentials [26] with an energy cutoff of 500 eV. Brillouin-zone k -point sampling was performed using the Monkhorst-Pack scheme with $10 \times 10 \times 10$ meshes for the calculation. The enthalpy of formation, ΔH_f at 0 K is described by Eq. (1).

$$\Delta H^\phi = E_{total}\phi - xE_{total}(M) - yE_{total}(B) \quad (M = Fe, W) \quad (1)$$

where ϕ is the boride M_xB_y in this ternary system, $E_{total}\phi$ is the total energy of M_xB_y at equilibrium lattice constants, $E_{total}(M)$ and $E_{total}(B)$ are the calculated total energies of the pure elemental constituents, respectively. When ϕ denotes the ternary boride, $E_{total}(M)$ should be changed to $E_{total}(Fe) + E_{total}(W)$. The reference states at 0K are BCC_A2 for Fe and W and Beta_Rhombo_B for B. Table 1 lists the crystal structures, and the experimental and calculated formation enthalpies ΔH , which are compared with the data reported in the literature for borides [27–38]. The calculated formation enthalpies of the ternary compounds (τ_1 , and τ_2) are used as the starting values for the parameters of the corresponding compounds in the optimization. The thermodynamic parameters of the binary borides are not assessed in this work, so the formation enthalpies of αWB , βWB , and W_2B_5 are calculated without considering the existence of the vacancy.

5.2. Thermodynamic modeling

5.2.1. Solution phases

The liquid phase is represented by a single sublattice, in which all the atoms are mixed. Its Gibbs energy is described as follows:

$$G_{Liquid} = \sum_i x_i^0 G_i + RT \sum_i x_i \ln x_i + \sum_{i,j} x_i x_j L_{i,j} + \sum_{i,j,k} x_i x_j x_k L_{i,j,k} \quad (i, j, k \\ = Fe, W, B) \quad (2)$$

In this system, the FCC, BCC and HCP are described using the substitutional solution model $(Fe, W)_a(B, Va)_c$ and the Gibbs energy can be expressed as:

$$G^\phi = \sum_i y_i \left(y_B^0 G_{i:B}^\phi + y_{Va}^0 G_{i:Va}^\phi \right) + aRT \sum_i y_i \ln y_i \\ + cRT (y_B \ln y_B + y_{Va} \ln y_{Va}) + y_W y_{Fe} (y_B L_{W,Fe:B} + y_{Va} L_{W,Fe:B}) \\ + y_B y_{Va} \sum_i y_i L_{i:B,VA} + G_{mag}^\phi \quad (i = Fe, W) \quad (3)$$

Here, y stands for the site fraction of component i in the relevant sublattice. ϕ represents the FCC, BCC, and HCP phases. a and c are the stoichiometric coefficients of each sublattice. R and T are the gas constant and the temperature in kelvin, respectively. ${}^0G_{i:Va}^\phi$ is the molar Gibbs energy of pure element i in the phase, and ${}^0G_{i:B}^\phi$ is the Gibbs energy of the hypothetical non-magnetic boride. $L_{W,Fe:B}^\phi$ and $L_{i:B,VA}^\phi$ are interaction parameters expressed by a Redlich-Kister polynomial [39], which will be evaluated in this work. G_{mag}^ϕ is the magnetic contribution to the Gibbs energy, which was assumed to be zero owing to a lack of experimental data.

5.2.2. Stoichiometric intermetallic compounds

There are 10 stable binary intermetallic compounds in the B-Fe-W system Fe_2B , FeB , μ , λ , W_2B , W_2B_5 , αWB , βWB , and $W_{1-x}B_3$, respectively. The solubilities of the third components in the binary B-Fe, B-W, and Fe-W phases were found to be small. No solubility of B was found in the Fe-W compounds, so the parameters of the Fe-W phases are from [20]. Therefore, the binary compounds Fe_2B , and FeB are treated as stoichiometric phases with two sublattices $(Fe, W)_a(B)_c$, and their Gibbs energy per mole is given as:

Table 3

Summary of thermodynamic parameters in the B-Fe-W system.

Phase and models	Thermodynamic parameters (J/mol)	Ref
Liquid: (B, Fe, W) _{1.0}	$0L_{B,Fe}^{Liquid} = -195392.478 + 82.88390754T$ (298.15-800 K) $-47176.286-9.7513909 T \cdot 5.9286591 \times 10^7 T^{-1}$ (800-6000 K) $1L_{B,Fe}^{Liquid} = +15272.916^2 L_{B,Fe}^{Liquid} = +46566.503$ $0L_{Fe,W}^{Liquid} = -19406.3 + 12.17^1 L_{Fe,W}^{Liquid} = +1743.7^2 L_{Fe,W}^{Liquid} = +4633.3$ $0L_{B,W}^{Liquid} = -148540 - 5.24T^1 L_{B,W}^{Liquid} = +11400 - 25.407T$ $0L_{Fe,W}^{Liquid} = -310000 + 62.85T$	[12]
BCC (Fe, W) ₁ (B, Va) ₃	$0L_{Fe,W;Va}^{BCC} = +18713.6 + 10.87^1 L_{Fe,W;Va}^{BCC} = -8860^2 L_{Fe,W;Va}^{BCC} = +7494.1$ $0G_{W,B}^{BCC} = +61450 + 20T + 3^0 G_B^{BETA_RHOMBO_B} + 0G_W^{BCC}$	[20]
FCC: (Fe, W) ₁ (B, Va) ₁	$0L_{Fe,W;Va}^{FCC} = +10944.5 + 5T$ $0L_{Fe,B;Va}^{FCC} = -57793.96 + 40.432377T$	[20]
FeB: (Fe, W) ₁ (B) ₁	$0G_{Fe,B}^{FeB} = -68308.455 + 3.9631668T + 0G_Fe^{BCC} + 0G_B^{BETA_RHOMBO_B}$ $0Tc_{Fe,B}^{FeB} = +600^0 \beta_{Fe,B}^{FeB} = +1.03$ $0L_{Fe,W;B}^{FeB} = -2360000 - 18T$	[12]
Fe ₂ B: (Fe) ₂ (B) ₁	$0G_{Fe,B}^{Fe2B} = -81226.188 + 3.1072761T + 2^0 G_Fe^{BCC} + 0G_B^{BETA_RHOMBO_B}$ $0Tc_{Fe,B}^{Fe2B} = +1018, 0\beta_{Fe,B}^{Fe2B} = +1.91$ $0L_{Fe,W;B}^{Fe2B} = -259300 - 36.5T$	[12]
α WB: (Fe, W) ₁ (B) ₁	$0G_{W,B}^{\alpha WB} = -84690 + 307.902T - 52.75T \ln(T) - 8.939 \times 10^{-4}T^2 + 787230T^{-1}$ – $5.38 \times 10^8 T^{-3}$ $0G_{W,Va}^{\alpha WB} = +49700 + 0G_W^{BCC0} G_{W,Va}^{\alpha WB} = -55520 + 16.89T$ $0L_{Fe,W;B}^{\alpha WB} = -48000 - 180T, 0L_{Fe,Va;B}^{\alpha WB} = -520000 + 200T$	[13]
β WB: (Fe, W) ₁ (B) ₁	$0G_{W,B}^{\beta WB} = -75528 + 304.168T - 52.75T \ln(T) - 8.939 \times 10^{-4}T^2 + 787230T^{-1}$ – $5.38 \times 10^8 T^{-3}$ $0G_{W,Va}^{\beta WB} = +59700 + 2.0T + 0G_W^{BCC0} L_{W,B,Va}^{\beta WB} = -74710 + 15.836T$ $0L_{Fe,W;B}^{\beta WB} = -9100 - 212T$	[13]
W ₂ B: (W) ₂ (B) ₁	$0G_{W,B}^{W2B} = -99580 + 487.255T - 84.432T \ln(T) - 4.77 \times 10^{-6}T^2 + 159100T^{-2}$ – $1.03 \times 10^{10} T^{-3}$ $0L_{Fe,W;B}^{W2B} = -390470$	[13]
W ₂ B ₅ : (W) ₂ (B, Va) ₅	$0L_{W,B}^{W2B5} = -195780 - 112.6T + 9.427T \ln(T) - 0.00704T^2 + 2^0 G_W^{BCC} + 5^0 G_B^{BETA_RHOMBO_B}$ $0L_{W,Va}^{W2B5} = +54750 + 2^0 G_W^{BCC0} L_{W,B,Va}^{W2B5} = -5640 + 73.61T$ $0L_{Fe,W;B}^{W2B5} = -500640$	[13]
W _{1-x} B ₃ : (W) ₂ (B) ₉	$0L_{W,B}^{W1-xB3} = -247380 - 51.84T + 2^0 G_W^{BCC} + 9^0 G_B^{BETA_RHOMBO_B}$	[13]
λ : (Fe, W) ₂ (Fe, W) ₁	$0G_{Fe,Fe}^{\lambda} = 3^0 G_{Fe,W}^{BCC} + 44130, 0G_{Fe,W}^{\lambda} = 2^0 G_{Fe}^{BCC} + 0G_W^{BCC} - 26803.6 + 13.5T$	[20]
μ : (Fe, W) ₁ W ₄ (Fe, W) ₂ (Fe, W) ₆	$0G_{Fe,W;Fe;Fe}^{\mu} = 9^0 G_{Fe}^{BCC} + 4^0 G_W^{BCC} - 76287.8 + 46.48T$ $0G_{W,W;Fe;Fe}^{\mu} = 8^0 G_{Fe}^{BCC} + 5^0 G_W^{BCC} + 78213$ $0G_{Fe;W;W;Fe}^{\mu} = 7^0 G_{Fe}^{BCC} + 6^0 G_W^{BCC} - 106224.1 + 48.93T$ $0G_{W;W;W;Fe}^{\mu} = 6^0 G_{Fe}^{BCC} + 7^0 G_W^{BCC} - 67688.98 + 80T^0 G_{Fe;W;Fe;W}^{\mu} = 3^0 G_{Fe}^{BCC} + 10^0 G_W^{BCC} + 430118$ $0G_{W;W;Fe;W}^{\mu} = 2^0 G_{Fe}^{BCC} + 11^0 G_W^{BCC} + 484188$ $0G_{Fe;W;W;W}^{\mu} = 0^0 G_{Fe}^{BCC} + 12^0 G_W^{BCC} + 375549$ $0G_{W;W;W;W}^{\mu} = 13^0 G_W^{BCC} + 469300$	[20]
τ_1 : Fe _{0.333} W _{0.333} B _{0.333}	$0G_{Fe;W;B}^{\tau_1} = -56796 + 6.03T + 0.333^0 G_{Fe}^{BCC} + 0.333^0 G_B^{BETA_RHOMBO_B} + 0.333^0 G_W^{BCC}$	[O*]
τ_2 : Fe _{0.2} W _{0.4} B _{0.4}	$0G_{Fe;W;B}^{\tau_2} = -64982 + 6.3T + 0.2^0 G_{Fe}^{BCC} + 0.4^0 G_B^{BETA_RHOMBO_B} + 0.4^0 G_W^{BCC}$	[O*]

 O^* - parameter optimized in this work.

$$G_{FeaBc} = \sum_i y_i y_B^0 G_{i:B} + aRT \sum_i y_i \ln y_i + cRT y_B \ln y_B + y_W y_{Fe} y_B L_{W,Fe:B} \left(i = Fe, W \right) \quad (4)$$

The solubilities of Fe in W₂B, α WB, and W₂B₅ at 1000 °C are approximately 2.8, 2.7 and 1.2 at%, respectively. To describe their solubility, the sublattice model (Fe, W)_m(B, Va)_n is used for W_mB_n compounds ($m = 2n = 0.667$ for W₂B, $m = n = 0.5$ for α WB, and

$m = 0.286, n = 0.714$ for W₂B₅). The Gibbs energies are expressed by the Eq. (2), except for $G_{mag}^{\varphi} = 0$. τ_1 and τ_2 were treated as the stoichiometric model (B)_x(Fe)_y(W)_z ($x = y = z = 0.333$ for τ_1 , $x = z = 0.4$, $y = 0.2$ for τ_2). Their Gibbs energy per mole of formula unit are expressed by Eq. (5).

$$G_{B_xFe_yW_z}^{\varphi} = x^0 G_B^{Beta-B} + y^0 G_{Fe}^{Bcc-A2} + z^0 G_W^{Bcc-A2} + a + bT \quad (5)$$

Here, the coefficients a and b are optimized in this work.

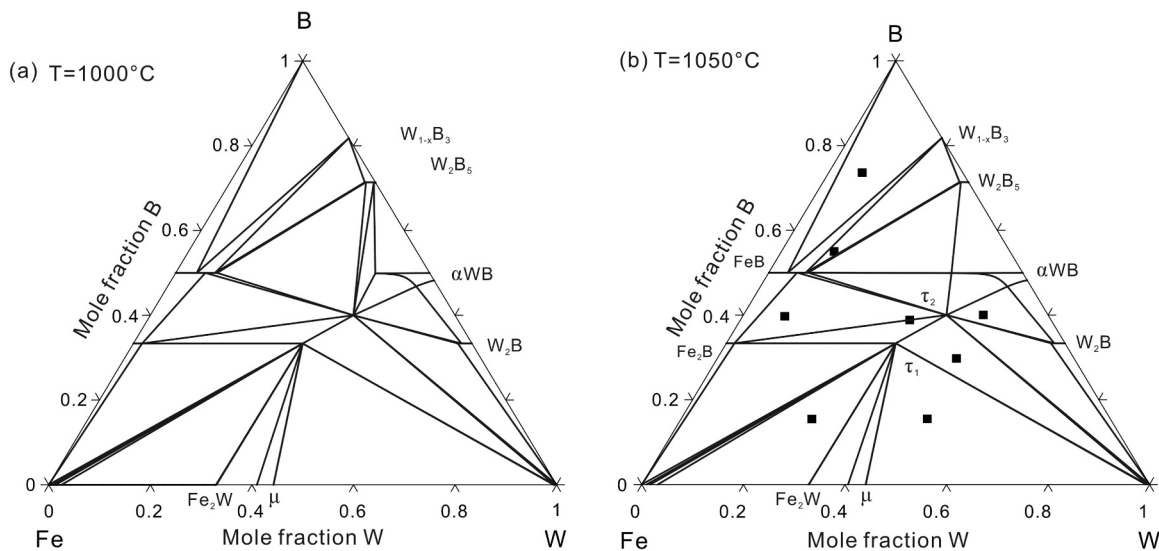


Fig. 7. Calculated isothermal sections of the B-Fe-W system (a) at 1000 °C and (b) at 1050 °C superimposed with the experimental data from Leithe-Jasper et al. [23].

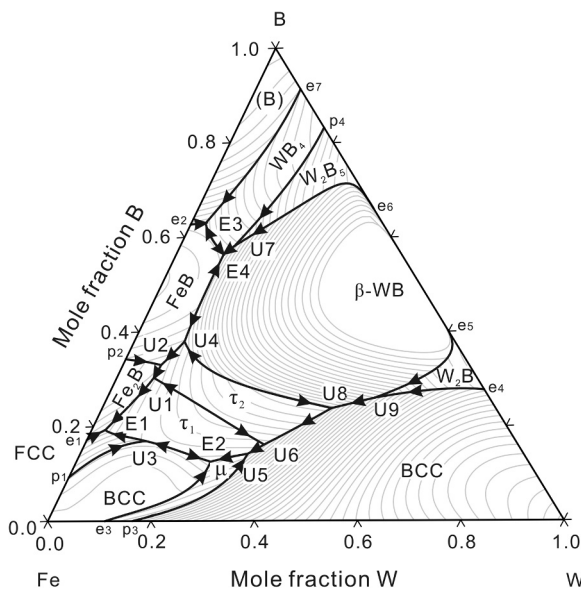


Fig. 8. Calculated liquidus surface projection of the B-Fe-W system over the whole composition range.

Table 4
Calculated invariant reactions with the available data in the B-Fe-W system.

Invariant reactions	Type	Temperature/°C	Liquid composition (at%)		
			B	Fe	W
L + W ₂ B ⇌ BCC + βWB	U9	2335.96	25.7	15.1	59.2
L + βWB ⇌ τ ₂ + BCC	U8	1772.39	21.5	35.5	43.0
L + W ₂ B ₅ ⇌ βWB + WB ₃	U7	1641.03	59.3	32.4	8.3
L + τ ₂ ⇌ BCC + τ ₁	U6	1504.83	15.0	51.1	33.9
L ⇌ FeB + βWB + W _{1-x} B ₃	E4	1534.73	57.0	36.2	6.8
L ⇌ (B) + FeB + W _{1-x} B ₃	E3	1475.15	63.1	35.4	1.5
L + BCC ⇌ μ + τ ₁	U5	1431.57	12.7	56.3	31.0
L + βWB ⇌ τ ₂ + FeB	U4	1414.78	36.2	57.1	6.7
L ⇌ τ ₁ + BCC + μ	E2	1382.81 1365 ^[O*]	10.7	65.1	24.2
L + BCC ⇌ τ ₁ + FCC	U3	1370.08	14.0	80.7	5.3
L + FeB ⇌ τ ₂ + Fe ₂ B	U2	1339.98	32.7	62.1	5.2
L + τ ₂ ⇌ τ ₁ + Fe ₂ B	U1	1322.04	29.5	65.6	4.9
L ⇌ τ ₁ + FCC + Fe ₂ B	E1	1188.24 1156 ^[O*]	18.2	80.4	1.4

[O*]: experimental value obtained in this work, otherwise the calculation.

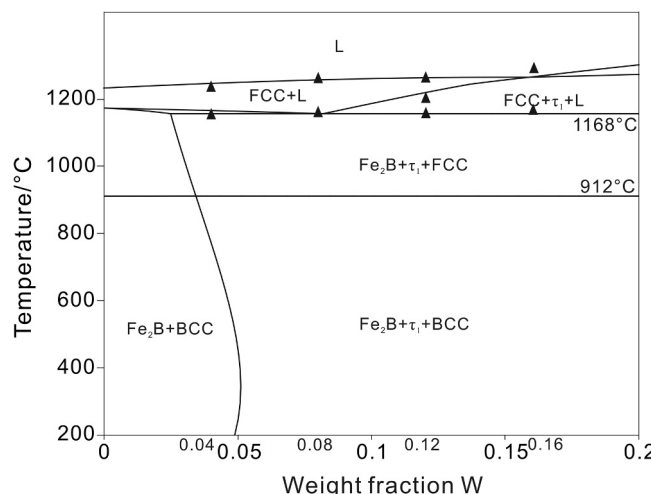


Fig. 9. Calculated vertical section with B fixed at 3.5 wt% compared with the DSC results from the present study.

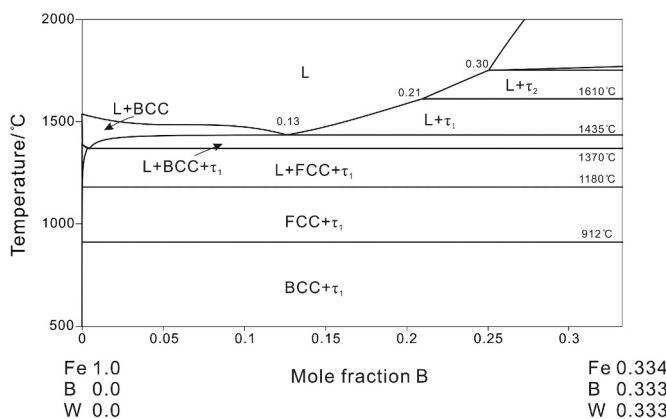


Fig. 10. Calculated vertical section diagram along the Fe- τ_1 join.

The experimental data obtained in this work were adopted for comparison.

To verify the applicability of the thermodynamic parameters obtained in this work, a partial vertical section with B fixed at 3.5 wt% was determined experimentally using SEM and DSC. Four as-cast Fe-3.5B alloys with various W contents (0, 4, 8, 12, and 16 wt%) were prepared and analyzed. The vertical section with B fixed at 3.5 wt% is derived and presented in Fig. 9, in which the experimental data obtained in this work are indicated by triangles. The primary solidification phase is solid solution FCC when the W content is less than 8 wt%.

τ_1 is a potential wear-resistant material. The vertical section of Fe- τ_1 can provide guidance for the preparation of WFeB-based cermets. Fig. 10 shows the calculated vertical section diagram along the Fe- τ_2 join (W: B = 1). The primary τ_1 phase is expected to form when the B content exceeds 21 at%, and liquid begins to form above 1170 °C. Because the experimental data for the B-Fe-W system are limited, further investigation is needed for clarification. The results of the present study might provide guidance for additional studies in future.

6. Conclusion

The liquidus projection of the B-Fe-W system in the Fe-rich region was determined experimentally. The primary phases are three terminal solid solutions (BCC-Fe, BCC-W, FCC), two binary intermetallics (Fe_2B , μ), and a ternary compound (τ_1 -WFeB). Two ternary eutectic reactions were confirmed in the investigated region $L \Leftrightarrow \gamma\text{-Fe} + \text{Fe}_2\text{B} + \tau_1$ at 1156 °C and $L \Leftrightarrow \mu + \tau_1 + \alpha\text{-Fe}$ at 1365 °C. The thermodynamic modeling of all the phases in the B-Fe-W ternary system was assessed. The calculated results are in good agreement with most of the experimental data.

Acknowledgments

This work is supported by National Natural Science Foundation of China (No. 51771160), National Science Foundation of China (No. 51471140), and Scientific Research Fund of Hunan Provincial Science and Technology Department (No. 2016JC2005).

References

- [1] K. Takagi, J. Solid State Chem. 179 (2006) 2809–2818.
- [2] B. Yuan, G.J. Zhang, Y.M. Kan, P.L. Wang, Int. J. Refract. Met. Hard Mater. 28 (2010) 291–296.
- [3] M. Komai, Y. Isobe, S. Ozaki, K. Takagi, J. Jpn. Soc. Powder Powder Metall. 40 (1993) 38–43.
- [4] J. Li, J. Li, C. Li, et al., Int. J. Refract. Met. Hard Mater. 46 (1) (2014) 80–83.
- [5] C. Li, Jialin Li, Jun Li, Ying Liu, Adv. Powder Technol. 26 (5) (2015) 1410–1416.
- [6] Y. Khan, E. Kneller, M. Sostarich, Z. Metallkd. 73 (1982) 624.
- [7] L. Battezzati, C. Antonione, J. Alloy Compd. 247 (1997) 164–171.
- [8] Y. Du, J.C. Schuster, Y.A. Chang, Z. Jin, B. Huang, Z. Metallkd. 93 (2002) 1157.
- [9] B. Hallemans, P. Wollants, J.R. Roos, Z. Metallkd. 85 (1994) 676.
- [10] K. Yoshitomi, Y. Nakama, H. Ohtani, M. Haeebe, ISIJ Int. 48 (2008) 835.
- [11] T.V. Rompaey, K.C. Hari Kumar, P.J. Wollants, Alloy. Compd. 334 (2002) 173.
- [12] M. Palumbo, G. Cacciamani, E. Bosco, et al., Calphad 25 (4) (2001) 625–637.
- [13] H. Duschanek, P. Rogl, J. Phase Equilibr. 16 (2) (1995) 150–161.
- [14] P. Villars, L.D. Calvert, Pearson's Handbook of Crystallographic Data for Intermetallic Phases, 2nd ed., ASM, Metals Park, Ohio, 1991.
- [15] W.P. Sykes, K.R. Van Horn, Trans. AIME 105 (1933) 198–214.
- [16] E.P. Sinha, W. Hume-Rothery, J. Iron Steel Inst. 205 (1967) 1145–1149.
- [17] P. Gustafson, Metall Trans., 18A (1987) 175–188.
- [18] A. Antoni-Zdziobek, T. Commeau, J.M. Joubert, Metall. Mater. Trans. A 44 (7) (2013) 2996–3003.
- [19] J.O. Andersson, P. Gustafson, Calphad 7 (1983) 317–326.
- [20] A. Jacob, C. Schmetterer, L. Singheiser, et al., Calphad 50 (2015) 92–104.
- [21] H. Haschke, H. Nowotny, F. Benesovsky, Mon. Chem. 97 (1966) 1459–1468.
- [22] P. Rogl, G. Effenberg, S. Ilyenok, Springer Materials, Landolt-Börnstein - Group IV Physical Chemistry 11D1 455, 2008.
- [23] A. Leithe-Jasper, H. Klesnar, P. Rogl, M. Komai, K.I. Takagi, J. Jpn. Inst. Met. 64 (2) (2000) 154–162.
- [24] G. Kresse, J. Furthmüller, Phys. Rev. B 54 (16) (1996) 11169–11186.
- [25] J.P. Perdew, K. Burke, M. Ernzerhof, Phys. Rev. L 77 (18) (1996) 3865–3868.
- [26] G. Kresse, D. Joubert, Phys. Rev. B 59 (3) (1999) 1758–1775.
- [27] P. Rogl, J.C. Schuster, ASM, Materials Park, OH, 1992, pp. 33–36.
- [28] P. Villars, L.D. Calvert, Pearson's Handbook of Crystallographic Data for Intermetallic Phases, 2nd ed., ASM, Metals Park, Ohio, 1991.
- [29] W. Jeitschko, Acta Crystallogr. 24B (1968) 930–934.
- [30] O.S. Gorelikin, A.S. Dubrovkin, O.D. Kolesnikova, N.A. Chirkov, Russ. J. Phys. Chem. 46 (1972) 431.
- [31] S. Owri, J. Wriyama, Trans. Jpn. Inst. Met. 21 (1980) 790.
- [32] S. Sato, O.J. Kleppa, Metall. Trans. B 13B (1982) 251.
- [33] V.P. Glushko, Thermal Constants of Substances Handbook, Akademiya Nauk SSSR, Moscow, 1974 (in Russian).
- [34] O. Kubaschewski, C.B. Alcock, P.J. Spencer, Materials Thermochemistry, Pergamon Press, New York, NY, 1993.
- [35] A.R. Miedema, J. Less-Common Met. 46 (1976) 67–83.
- [36] (a) V.Y. Leonidov, O.M. Gaisinskaya, V.S. Pervov, S.S. Ordan'yan, L.V. Kudryasheva, Zh. Fiz. Khim. 52 (1976) 313–316 (in Russian); (b) TR, Russ. J. Phys. Chem. 52 (1978) 172–174.
- [37] S. Meschel, O.J. Kleppa, J. Chim. Phys. 90 (1993) 349–354.
- [38] L. Kaufman, B. Uhrenius, D. Birnie, K. Taylor, Calphad 8 (1984) 25–66.
- [39] O. Redlich, A. Kister, Ind. Eng. Chem. 40 (1948) 345.